# GENETIC ALGORITHM FOR SPACE DEBRIS AND SPACE OBJECTS ATTITUDE MOTION RECONSTRUCTION THROUGH OPTICAL MEASUREMENTS

**Lorenzo Cimino[(1)], Lorenzo Mariani[(1)], Simone Varanese(1), Gaetano Zarcone[(1)], Mascia Bucciarelli[(1)], Mirko Cerci[(1)], Shariar Hadji Hossein[(1)], Matteo Rossetti[(1)], Fabrizio Piergentili[(1)]**

*[(1)] Department of Mechanical and Aerospace Engineering (DIMA), University of Rome "La Sapienza"; cimino.1785896@studenti.uniroma1.it, simone.varanese@uniroma1.it, lorenzo.mariani@uniroma1.it, gaetano.zarcone@uniroma1.it, bucciarelli.1792406@studenti.uniroma1.it, cerci.1460361@studenti.uniroma1.it, shariar.hadjihossein@gmail.com, rossetti.1821458@studenti.uniroma1.it, fabrizio.piergentili@uniroma1.it*

## ABSTRACT

Space debris has recently become a major problem in the planning and execution of space missions. Due to the recent widespread placement of satellite mega-constellations in Low Earth Orbits (LEO), where most of the catalogued debris is located, the need to monitor such uncontrolled objects and maintain an up-to-date catalogue has increased. Moreover, estimating the attitude motion of a space object is fundamental to improving methods for orbit determination and supporting eventual Active Debris Removal (ADR) missions. The Sapienza Space System and Space Surveillance Laboratory (S5Lab), whose researchers have years of experience in space debris detection, operates an extensive observation network that can exploit different observation strategies. This paper illustrates the reconstruction of an object's attitude motion from its light curve, which can be extracted using scientific Complementary Metal-Oxide Semiconductor (sCMOS) sensors installed on high-slew rate telescopes. The method is based on a comparison between the object's actual light curve and a synthetic curve created by changing the initial conditions for the attitude motion, considering the observer's motion, the Sun's position, the object's position and its 3D model. A genetic algorithm is used to create multiple synthetic light curves by varying the initial conditions for the attitude motion until one of them matches the observed one. In addition to extracting the light curves and reconstructing the attitude, observational strategies for acquiring light curves are discussed. Finally, the results of the investigation of potentially hazardous debris are presented.

## 1 INTRODUCTION

Easy and safe access to near-Earth space is essential to advance and facilitate both human activities on Earth and scientific research in space. Over the past decade, however, space has become increasingly crowded due to the dramatic increase in payloads launched and released in Earth orbit. Fig. 1 shows the exponential growth in launch traffic for Low Earth Orbit (LEO) payloads over the years. These peaks in recent years are due to the increasing use of space not only by public space agencies but also by private companies.

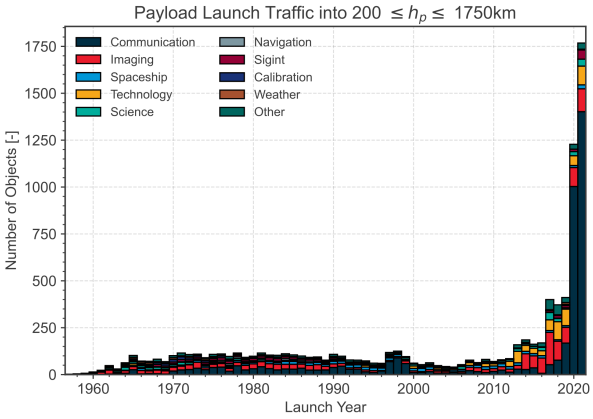


*Figure 1. Payload launched over the years [2]*

The population of artificial space objects can be divided into two categories: active satellites or spacecraft and space debris. The latter are defined by the Inter-Agency Space Debris Coordination Committee (IADC) as "all man-made objects, including parts and elements thereof, that are in Earth orbit or re-entering the atmosphere and are non-functional" [1].

All trackable objects in Earth orbit are continuously catalogued by the North American Aerospace Defence (NORAD). So far, the majority of these objects are debris (about 60%), followed by active satellites from the new mega-constellations established in recent years, such as Starlink and OneWeb.

Focusing exclusively on space debris, the number of these objects is steadily increasing. Even if no more launches take place, the number of space debris objects is estimated to continue to increase, as shown in Fig. 2.

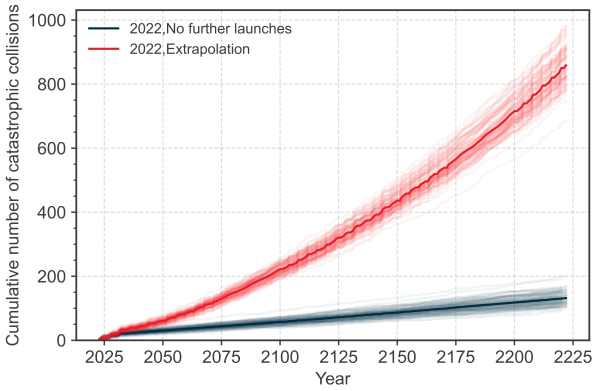


*Figure 2. The creation of space debris would not be stopped even by stopping all further launches [2]*

The creation of space debris can occur for a variety of reasons. The main cause is on-orbit fragmentation events [2,3], mainly caused by the remaining fuel on board the spacecraft or in the upper stage tanks and pipelines. The space environment can damage the mechanical and physical integrity of the parts, which can lead to mixing of the propellant components and thus to an explosion. Fig. 3 shows the causes of fragmentation events and their relative proportion over the last 10 years. It is estimated that these events have produced about 1 million fragments larger than 1 cm [2], increasing the population of space objects. Therefore, collisions are expected to be the main cause of debris generation in the coming years [4]. Space debris is also generated by international anti-satellite (ASAT) tests.

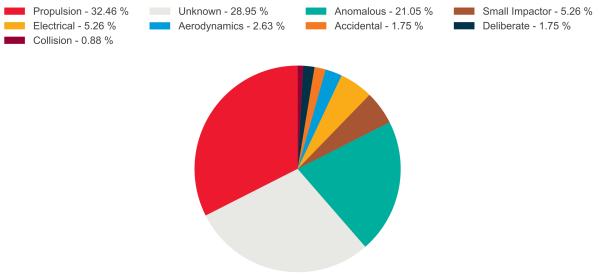


*Figure 3. Fragmentation event causes over the last 10 years [2]*

Space debris is dangerous for two main reasons: first, it can collide with operational satellites, resulting in the loss of the satellite and the creation of new debris clouds; and second, it can re-enter the atmosphere, especially if it is in LEO. Since a space debris is not manoeuvrable, it will gradually lower its orbit and re-enter the atmosphere due to atmospheric drag. Uncontrolled re-entry can pose a hazard to both humans and ground-based facilities. To cope with the increasing number of space objects and to ensure safe space missions, new programmes and research areas, such as Space Traffic Management (STM), have emerged over the years [5]. In order to avoid unwanted collisions with manoeuvrable spacecraft, great efforts have been made in recent decades to maintain an updated catalogue of debris objects as part of the Space Surveillance and Tracking (SST) programme [6]. The position of these objects is tracked using both active observation methods (e.g. radar and lasers) and passive methods (e.g. optical sensors and telescopes).

Knowledge of the dynamics of the attitude of space debris and, more generally, of space objects is crucial for numerous applications. For example, in the context of Active Debris Removal (ADR) missions, an operational spacecraft needs to know the exact attitude of the debris in order to capture it [7]. Instead, in case of the re-entry of a space object, the attitude dynamics has a strong influence on the trajectory of the object. This is because the drag acting on the object is determined by its ballistic coefficient, which is a function of the object's orientation in space. This plays a crucial role in estimating the point of impact of the object on the ground [8]. With a ground-based optical system, it is possible to reconstruct the attitude motion of the object by analysing its observed light curve, that is the variation over time of the sunlight reflected from the object itself. The observed light curve is compared with several synthetic curves automatically generated by a specially developed software.

This paper shows the results of several tests performed with an algorithm developed within the Sapienza Space Systems and Space Surveillance Laboratory (S5Lab) [9-12]. Before proceeding with the use of observed light curves, several tests were performed with simulated light curves to prove the functionality of the software and to evaluate the advantages and disadvantages of different optimisation algorithms. The software creates a synthetic light curve, taking into account the position of the observer, the position of the Sun, the object's position and its 3D model. Multiple light curves are generated until one matches the reference curve. The approach described in the following sections was applied to three objects, using different conditions for the initial attitude.

## 2 TARGET CHARACTERIZATION

Three different space objects with different physical properties were considered to show how the shape of a space object affects the reflection of sunlight and thus the process of reconstructing its attitude. The following three LEO objects were considered:

- EO-1, an inactive satellite with a solar panel
- Jason 2, an inactive satellite with two solar panels
- Delta II, the upper stage of the Delta expendable launch system

The main orbital characteristics of the selected objects are shown in Tab. 1.

*Table 1. Orbital characteristics of the selected objects*

| Object | ID | Inclin. | Perigee | Apogee |
|---|---|---|---|---|
| *Jason 2* | 33105 | 66.0 ° | 1312 km | 1323 km |
| *EO-1* | 26619 | 97.9 ° | 676 km | 691 km |
| *Delta II* | 20453 | 35.6 ° | 417 km | 772 km |

The 3D model of each object is shown in the following figures: Fig. 4 shows the 3D model of Jason 2, Fig. 5 of EO-1 and Fig. 6 of Delta II. These models were taken from [13] and are needed for the reconstruction of the attitude motion of the object.

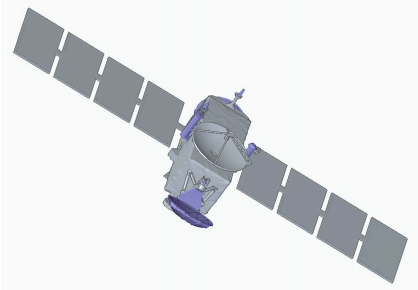

*Figure 4. 3D model of Jason 2*

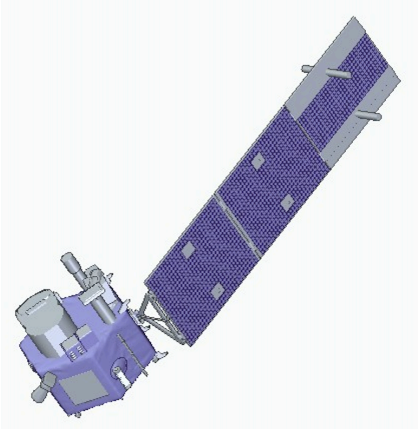

*Figure 5. 3D model of EO-1*

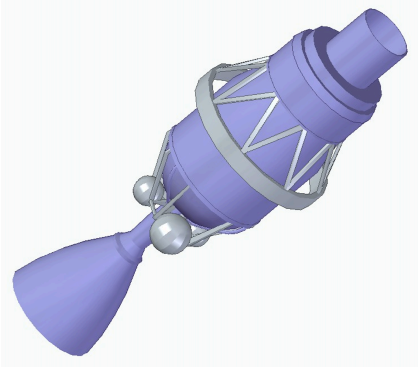

*Figure 6. 3D model of Delta II*

## 3 LIGHT CURVE

A light curve is the variation in brightness of a celestial object over a period of time. The object's brightness can be measured either as apparent or absolute magnitude. The apparent magnitude is the brightness of the object as it appears in the night sky from Earth, while the absolute magnitude measures the intrinsic luminosity emitted from the object. Different parts of the spectrum can be used to acquire light curves.

Originally, light curves were used to study the physical properties of celestial objects such as asteroids, planets, stars, and galaxies. For example, the rotation period of a celestial body can be computed from its light curve, or stars can be classified using light curves. In recent years, light curves have been widely used to determine the rotation rate of artificial objects such as satellites and space debris [12].

Light curves can be extracted from high frame rate videos taken with scientific Complementary Metal-Oxide Semiconductor (sCMOS) sensors mounted on powerful telescopes. A typical procedure is described in [12]. Fig. 7 shows the light curve of the SL-14 Rocket Body observed by RESDOS, one of the S5Lab telescopes [11]. The rotation rate of the observed object can be deduced from the strong periodic signature.

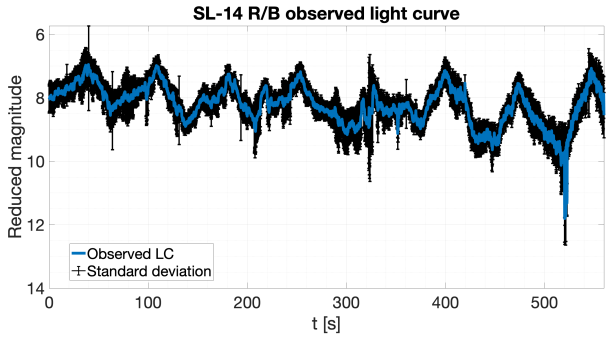


*Figure 7. Light curve of SL-14 R/B, NORAD ID 18340, observed on July 17, 2022, from RESDOS [11]. The cyan line represents the mean value of the magnitude, while the black area represents the standard deviation. The magnitude is reduced with respect to the range from the observatory.*

Light curves can also be simulated for a variety of purposes, such as studying the effect of an object's attitude motion on its brightness and estimating the effects of reflected light in the night sky.

Since a light curve depends on the amount of sunlight reflected from an object, the following inputs must be considered when creating a simulated light curve:

- Position of the Sun
- Position of the object
- 3D model of the object

- Position of the observer

In addition, the three angular velocities and three Euler angles in the body reference frame are required as initial conditions for the attitude dynamics. In this way, the light curve of the object can be generated during a simulated pass over a specific observatory on the ground.

## 4 FOURIER METHOD

The goal of the optimisation algorithm is to determine the initial conditions for the attitude of the object, which is defined by three angular positions and three angular velocities with respect to the central axes of inertia. The solution space thus has six dimensions. In order to minimise the extremely high computational costs, which can be up to days, a procedure for minimising the solution space is required. To speed up the procedure, an a priori analysis can be performed based on the study of the light curve frequencies.

The cut-off values for the angular velocities, which serve as inputs to the algorithm, are determined using a method based on the Fast Fourier Transform (FFT) [14]. The first five frequencies of the simulated light curves with the highest frequency content are identified by evaluating their FFT. These frequencies are defined as carrier frequencies.

The minimum and maximum frequencies of the solution space can be determined from the identified carrier frequencies. Indeed, numerous simulations have shown that the natural frequency of the object falls within the frequency range considered, which can be used to narrow down the space of possible solutions.

The natural frequency of a satellite is given by:

$$f_{sat} = \frac{1}{2\pi}\sqrt{\omega_1^2 + \omega_2^2 + \omega_3^2} \qquad (1)$$

As an example, the simulated light curves of Jason 2 are shown in Fig. 8. The plots show cases of pure rotation about a single central axis of inertia, all with an initial condition of 0.03 $s^{-1}$ for the angular velocity.

Considering the light curves shown in Fig. 8, the frequency spectrum can be reconstructed using the FFT, as shown in Fig. 9, where the determined bandwidth is also given. The latter allows the solution space to be narrowed down.

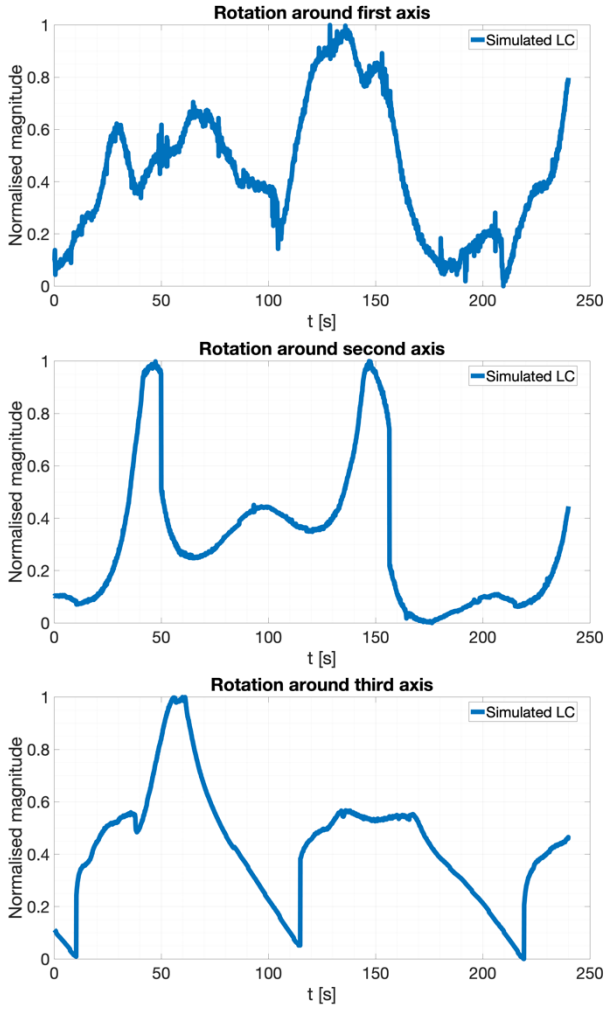


*Figure 8. Simulated light curves obtained assuming pure rotation about a single axis as initial condition. The brightness is normalised between 0 and 1. The integration time is 240 seconds.*

## 5 LIGHT CURVE INVERSION AND OPTIMISATION ALGORITHMS

The inversion of a light curve involves the recovery of the attitude parameters of an object in orbit. In this study, the procedure was adapted to work with light curves from optical measurements. As mentioned earlier, knowing and predicting the attitude of an object is crucial in problems involving uncontrollable and non-manoeuvrable bodies, such as space debris, to improve the understanding of their motion dynamics in special cases, such as atmospheric re-entry.

In this work, simulated observations were used to test a routine for inverting light curves to determine the attitude parameters of a target body at a given time.

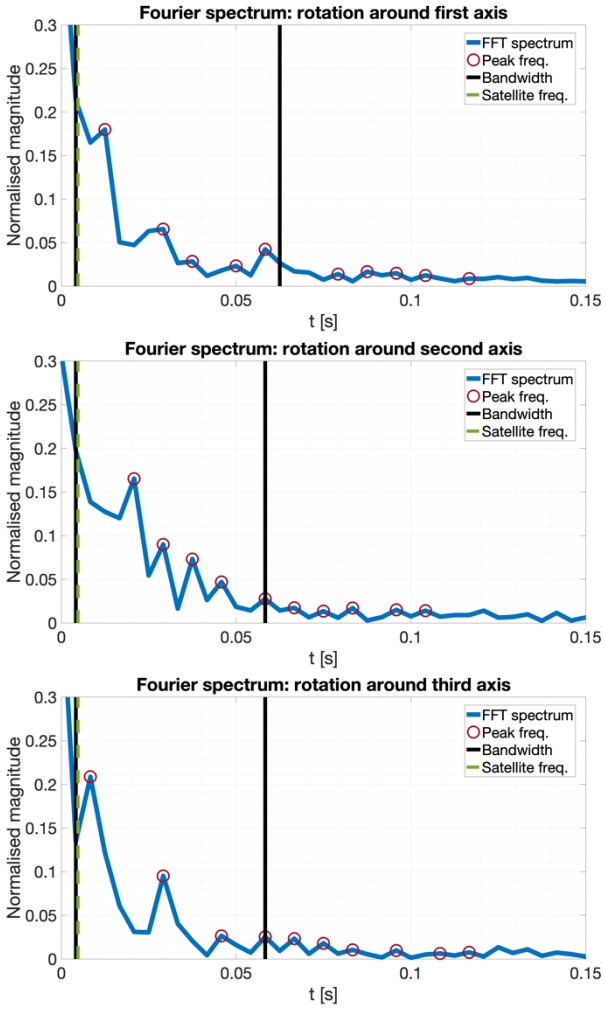


*Figure 9. Frequency spectrum corresponding to the light curves in Fig. 8. After determining the bandwidth using the first five carrier frequencies, the graph shows that the satellite's natural frequency falls within this range.*

The first step in inverting a light curve is to develop software that can simulate optical observations. An observation is primarily determined by the position of the Sun, the position of the object and the relative position of the observer. In order to conduct a successful observation, the visibility conditions must be fulfilled. These include the observer being in the dark, the object being illuminated by the Sun and the object being above the observer's horizon.

The software requires the following inputs to generate a simulated observation:

- Two-Line Elements (TLE) [15] set of the object is used to calculate its position in time using an SGP4 propagator [16]
- 3D model of the object, useful to retrieve its inertia matrix, is needed for the integration of the Euler equations, and to know the reflection properties of the object
- Six initial conditions for the attitude: the three Euler angles and the corresponding angular velocities
- Position of the observer
- Ephemeris of the Sun
- Start and end times of the passage

The above parameters can be used to create a simulated light curve of an object passing over an observatory, as shown in Fig. 8. The software also includes a graphics engine that displays the object's passage over the observatory over time, as shown in Fig. 10.

Once a simulated observation has been created, the attitude reconstruction process can be run. The core of the process is an optimisation algorithm that computes the same initial conditions that were to generate the simulated reference light curve.

The bounded domain of initial conditions identified by the Fourier approach described in Section 4, i.e. the space of solutions, is passed to the optimisation process along with the reference light curve. At each iteration, the optimisation process compares the reference light curve with a new simulated light curve obtained with a set of initial conditions selected by the algorithm during the exploration of the solution space. The goal of this process is to evaluate and minimise an index called energy so that the closest simulated light curve to the reference curve is found. The results of the process are the initial conditions associated with the simulated light curve that best matches the reference curve.

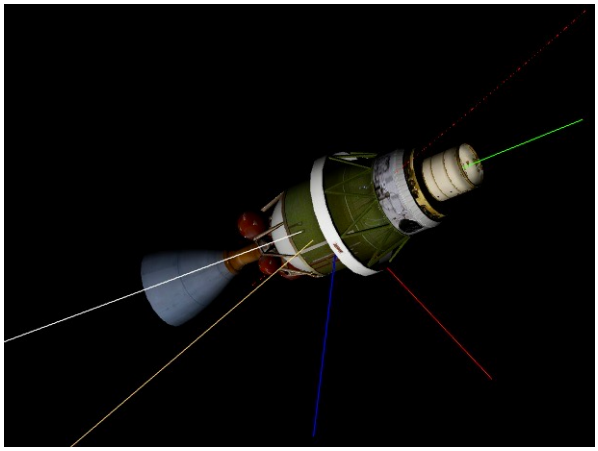

*Figure 10. Rendering of Delta II during the simulation of its passage over of the observatory. The green, blue, and red axes are the central axes of inertia.*

Different optimisation algorithms can be used. In this work, a Multi-Objective Particle Swarm Optimisation (MOPSO) [17] and a Multi-Objective Genetic Algorithm (MOGA) [18] were used. The following is a brief

introduction to these methods.

The population-based stochastic optimisation method, known as Particle Swarm Optimisation (PSO), was inspired by the flocking behaviour of birds. The iterative multi-objective optimisation method, known as MOPSO, is close to evolutionary computational methods such as Genetic Algorithms (GA). It is less robust than GA, but compensates for this with a faster convergence speed, making it a useful GA alternative when evaluations require more computational effort. Although it is an exploratory method, the MOPSO algorithm manages to find an acceptable suboptimal solution. The main problem with using this approach is the high computational cost of finding an optimal solution.

MOGA, on the other hand, is a multi-objective genetic algorithm that performs optimisation using a multi-search elitism. Since MOGA is an exploratory algorithm, it explores the entire space of possible solutions rather than converging to a local minimum. The MOGA optimisation algorithm is very powerful and reliable. However, it has some problems, such as high computational costs and the tendency to converge to local bounds, which becomes a limit after many iterations.

## 6 SIMULATIONS AND RESULTS

The objects presented in Section 3 were used as test cases. Several simulations were performed to determine the initial attitude parameters used to generate the simulated reference light curves. The following sections show the results of the optimisation process with the different algorithms used.

### 6.1 Case study: Jason 2

A coupled rotation along the first and third axes was chosen as initial condition to generate the reference light curve of Jason 2. The results of the optimisation process obtained with a MOPSO and a MOGA are shown in Fig. 11 and Fig. 12. Tab. 2 reports a summary of the numerical results found for both cases.

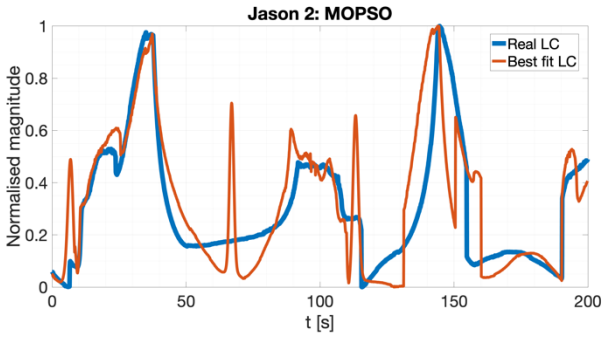


*Figure 11. Optimisation of Jason 2's light curve obtained using a MOPSO*

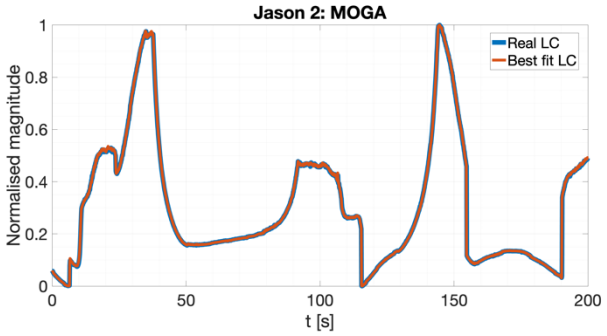


*Figure 12. Optimisation of Jason 2's light curve obtained using a MOGA*

*Table 2. Numerical results for Jason 2. The first column reports the initial attitude that determines the reference light curve. Then the results and corresponding errors obtained with a MOPSO and a MOGA are reported.*

| | Ref. | MOPSO | Error MOPSO | MOGA | Error MOGA |
|---|---|---|---|---|---|
| $\omega_1$ *[rad/s]* | 0.05 | 0.048 | 0.002 | 0.049 | 0.01 |
| $\omega_2$ *[rad/s]* | 0 | -0.023 | 0.023 | 0 | 0 |
| $\omega_3$ *[rad/s]* | 0.05 | 0.045 | 0.005 | 0.05 | 0 |
| $\theta_1$ *[rad]* | 0 | -0.046 | 0.046 | -0.057 | 0.057 |
| $\theta_2$ *[rad]* | 0 | -0.168 | 0.168 | -0.259 | 0.259 |
| $\theta_3$ *[rad]* | 1.58 | 1.57 | 0.01 | 1.581 | -0.001 |

### 6.2 Case study: EO-1

A random rotation was chosen as initial condition to generate the reference light curve of EO-1. The results of the optimisation process obtained with a MOPSO and a MOGA are shown in Fig. 13 and Fig. 14. Tab. 3 reports a summary of the numerical results found for both cases.

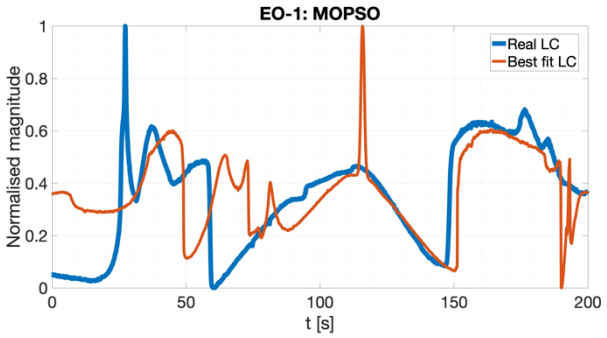


*Figure 13. Optimisation of EO-1's light curve obtained using a MOPSO*

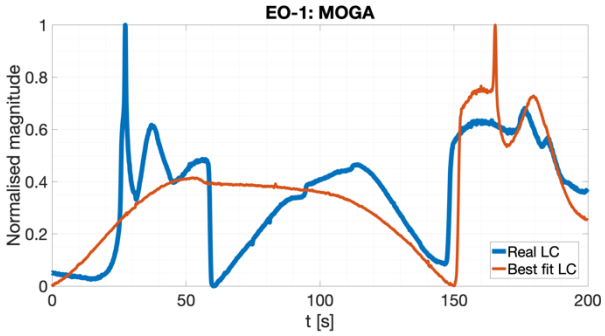


*Figure 14. Optimisation of EO-1's light curve obtained using a MOGA*

*Table 3. Numerical results for EO-1. The first column reports the initial attitude that determines the reference light curve. Then the results and corresponding errors obtained with a MOPSO and a MOGA are reported.*

| | Ref. | MOPSO | Error MOPSO | MOGA | Error MOGA |
|---|---|---|---|---|---|
| $\omega_1$ *[rad/s]* | 0.01 | -0.001 | 0.011 | 0.014 | 0.004 |
| $\omega_2$ *[rad/s]* | 0.002 | 0.019 | -0.017 | 0.007 | 0.005 |
| $\omega_3$ *[rad/s]* | 0.05 | -0.025 | 0.075 | -0.006 | 0.056 |
| $\theta_1$ *[rad]* | 1.75 | -1.333 | 3.083 | 1.7 | 0.05 |
| $\theta_2$ *[rad]* | 0.1 | -0.126 | 0.226 | 0.147 | -0.047 |
| $\theta_3$ *[rad]* | -1.55 | 0.787 | -2.337 | -1.516 | -0.034 |

### 6.3 Case study: Delta II

A random rotation was chosen as initial condition to generate the reference light curve of Delta II. The results of the optimisation process obtained with a MOPSO and a MOGA are shown in Fig. 15 and Fig. 16. Tab. 4 reports a summary of the numerical results found for both cases.

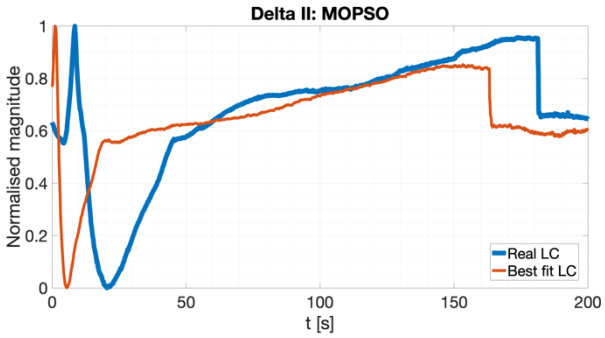


*Figure 15. Optimisation of Delta II's light curve obtained using a MOPSO*

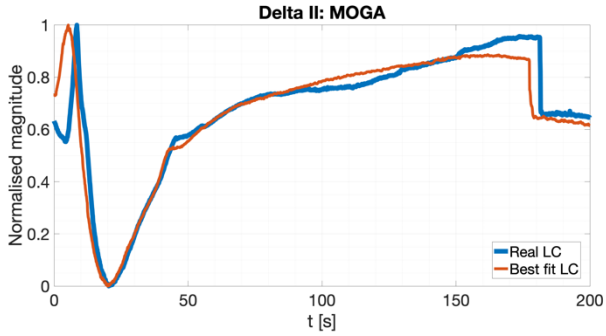


*Figure 16. Optimisation of Delta II's light curve obtained using a MOGA*

*Table 4. Numerical results for Delta II. The first column reports the initial attitude that determines the reference light curve. Then the results and corresponding errors obtained with a MOPSO and a MOGA are reported.*

| | Ref. | MOPSO | Error MOPSO | MOGA | Error MOGA |
|---|---|---|---|---|---|
| $\omega_1$ *[rad/s]* | 0.08 | 0.014 | 0.066 | 0.012 | 0.068 |
| $\omega_2$ *[rad/s]* | 0.002 | 0.007 | -0.005 | 0.004 | -0.002 |
| $\omega_3$ *[rad/s]* | 0.01 | 0.002 | 0.008 | 0.0005 | 0.0095 |
| $\theta_1$ *[rad]* | 1.6 | 1.57 | 0.03 | 1.609 | -0.009 |
| $\theta_2$ *[rad]* | 1.35 | 1.537 | -0.187 | 1.457 | -0.107 |
| $\theta_3$ *[rad]* | -1.35 | 1.516 | -2.866 | -1.388 | 0.038 |

The three objects exhibit significantly different light curves due to their shape, as shown in the previous figures. Since Jason 2 and EO-1 are equipped with solar panels, they have the most complex light curves. In contrast, the light curve of Delta II has a simpler shape and exhibits only one peak. In each case, the combined actions of the optimisation algorithm and the light curve generator are successful in determining the original initial conditions for the attitude.

## 7 CONCLUSIONS

A typical process for inverting a light curve was broken down into its critical parts. In this study, synthetic light curves were used instead of real light curves to validate the attitude reconstruction software developed by researchers at S5Lab. Three different space objects orbiting the Earth were the focus of the simulations. The results show how the use of different optimisation methods for the attitude reconstruction problem can lead to different results. In each case, the genetic algorithm MOGA provided a more accurate estimate of the initial conditions that led to the creation of the reference light

curve. This is true for both the angular positions and the angular velocities. On the other hand, the MOPSO performs well in estimating the angular velocities but poorly in determining the angular positions. However, the latter can still be used together with another optimisation algorithm in a combined approach. Thus, the results show the effectiveness of the considered approach for reconstructing the attitude of objects with different shapes using optical observations alone. The results obtained using observable measurements can be very promising.

Future developments concern the use of a MOPSO together with a MOGA and the integration of other optimisation algorithms to increase the accuracy of the solution. Then, the method can be applied to real cases of objects re-entering the atmosphere using their observed light curve.

## 8 REFERENCES


1. IADC-02-01 Space Debris Guidelines Rev_3, 2021. IADC (iadc-home.org). Accessed on 2022-01-03
2. Esa's annual space environment report, 2022. https://www.sdo.esoc.esa.int/environment_report/Space_Environment_Report_latest.pdf. Accessed on 2022-01-03
3. G. Zarcone, M. Rossetti, S. Hadji Hossein, F. Piergentili. A graphical method for the analysis of a satellite's in-orbit breakup through optical observations. Advances in Space Research, Volume 70, Issue 4, 2022, Pages 1048-1061, ISSN 0273-1177, https://doi.org/10.1016/j.asr.2022.05.032.
4. Kessler, Donald J., and Burton G. Cour-Palais. "Collision frequency of artificial satellites: The creation of a debris belt." Journal of Geophysical Research: Space Physics 83.A6 (1978): 2637-2646.
5. https://defence-industry-space.ec.europa.eu/eu-space-policy/eu-space-programme/eu-approach-space-traffic-management_en Accessed on 2022-01-03
6. https://www.eusst.eu Accessed on 2022-01-03
7. Aslanov V.S., Ledkov A.S., Fuel costs estimation for ion beam assisted space debris removal mission with and without attitude control, (2021) Acta Astronautica, 187, pp. 123 - 132, DOI: 10.1016/j.actaastro.2021.06.028.
8. Crowther, R. "Re-entry aerodynamics derived from space debris trajectory analysis." Planetary and space science 40.5 (1992): 641-646.
9. F. Piergentili et al., "Satellite early identification through LED observations: First in-orbit results from WildTrackCube-SIMBA," Acta Astronautica, vol. 193, pp. 163–172, Apr. 2022, doi: 10.1016/j.actaastro.2022.01.014.
10. Hadji Hossein, S., Cimino, L., Rossetti, M., Zarcone, G., Mariani, L., Bucciarelli, M., Seitzer, P., Santoni, F., Di Cecco A., Piergentili F., Photometric characterization of Starlink satellite tracklets using RGB filters, Advances in Space Research, 2022, ISSN 0273-1177, https://doi.org/10.1016/j.asr.2022.07.082.
11. Hadji Hosein, S. et al., 2020. Sapienza Space debris Observatory Network (SSON): A high coverage infrastructure for space debris monitoring. Journal of Space Safety Engineering 7, 30–37.
12. Piergentili, F.; Zarcone, G.; Parisi, L.; Mariani, L.; Hossein, S.H.; Santoni, F. LEO Object's Light-Curve Acquisition System and Their Inversion for Attitude Reconstruction, Aerospace 2021, 8(1), 4; DOI:10.3390/aerospace8010004.
13. https://nasa3d.arc.nasa.gov/models Accessed on 2022-01-03
14. Brigham, E. Oran. The fast Fourier transform and its applications. Prentice-Hall, Inc., 1988.
15. Vallado, D.; Cefola, P. «Two-line element sets-Practice and use». In Proceedings of the 63rd International Astronautical Congress, Naples, Italy, 1–5 October 2012; IAF: Paris, France, 2012. IAC-12,C1,6,12,x13640. Volume 7, pp. 5812–5825.
16. Vallado, D.A.; McClain,W.D. Fundamentals of Astrodynamics and Applications, 3rd ed.; Microcosm Press/Springer: Hawthorne, CA, USA, 2007.
17. Coello, CA Coello, and Maximino Salazar Lechuga. "MOPSO: A proposal for multiple objective particle swarm optimization." Proceedings of the 2002 Congress on Evolutionary Computation. CEC'02 (Cat. No. 02TH8600). Vol. 2. IEEE, 2002.
18. Murata, Tadahiko, and Hisao Ishibuchi. "MOGA: multi-objective genetic algorithms." IEEE international conference on evolutionary computation. Vol. 1. Piscataway, NJ, USA: IEEE, 1995.